

3D bioactive cell-free-scaffolds for in-vitro/in-vivo capture and directed osteoinduction of stem cells for bone tissue regeneration

Mamatali Rahman^{b,c}, Xue-Liang Peng^a, Xiao-Hong Zhao^a, Hai-Lun Gong^a, Xiao-Dan Sun^{d,e}, Qiong Wu^{b,c,**}, Dai-Xu Wei^{a,*}

^a Key Laboratory of Resource Biology and Biotechnology in Western China, Ministry of Education, School of Medicine, Department of Life Sciences and Medicine, Northwest University, Xi'an, 710069, China

^b MOE Key Laboratory of Bioinformatics, Center for Synthetic and System Biology, Tsinghua University, Beijing, 100084, China

^c School of Life Sciences, Tsinghua University, Beijing, 100084, China

^d State Key Laboratory of New Ceramics and Fine Processing, School of Materials Science and Engineering, Tsinghua University, Beijing, 100084, China

^e Key Laboratory of Advanced Materials of Ministry of Education of China, School of Materials Science and Engineering, Tsinghua University, Beijing, 100084, China

ARTICLE INFO

Keywords:

Soybean lecithin
Bioactive material
Cell-free scaffold
BMP2
Cell-capture
Ossification

ABSTRACT

Hydrophilic bone morphogenetic protein 2 (BMP2) is easily degraded and difficult to load onto hydrophobic carrier materials, which limits the application of polyester materials in bone tissue engineering. Based on soybean-lecithin as an adjuvant biosurfactant, we designed a novel cell-free-scaffold of polymer of poly(ϵ -caprolactone) and poly(lactide-co-glycolide)-co-polyetherimide with abundant entrapped and continuously released BMP2 for *in vivo* stem cell-capture and *in situ* osteogenic induction, avoiding the use of exogenous cells. The optimized bioactive osteo-polyester scaffold (BOPSC), i.e. SBMP-10SC, had a high BMP2 entrapment efficiency of 95.35%. Due to its higher porosity of 83.42%, higher water uptake ratio of 850%, and sustained BMP2 release with polymer degradation, BOPSCs were demonstrated to support excellent *in vitro* capture, proliferation, migration and osteogenic differentiation of mouse adipose derived mesenchymal stem cells (mADSCs), and performed much better than traditional BMP-10SCs with unmodified BMP2 and single polyester scaffolds (10SCs). Furthermore, *in vivo* capture and migration of stem cells and differentiation into osteoblasts was observed in mice implanted with BOPSCs without exogenous cells, which enabled allogeneic bone formation with a high bone mineral density and ratios of new bone volume to existing tissue volume after 6 months. The BOPSC is an advanced 3D cell-free platform with sustained BMP2 supply for *in situ* stem cell capture and osteoinduction in bone tissue engineering with potential for clinical translation.

1. Introduction

Mostly based on ordered incorporation of seed-cells, scaffolds made of biomaterials and osteogenic signaling factors, bone tissue engineering is one of the most effective methods for regeneration of various bones, including weight-bearing bones and non-load-bearing bones [1–3]. The use of natural or synthetic scaffolds for bone regeneration has been considered as a promising alternative to natural bone grafts [4–9].

Due to their excellent spatial plasticity, polyesters were used to

produce various scaffolds for bone tissue engineering *via* foaming [10–12], 3D-printing [13–15] and spinning [16–18]. The related polyesters mainly include polylactide (PLA) [10,19–21], poly(ϵ -caprolactone) (PCL) [14,22–24], poly(lactide-co-glycolide) (PLGA) [25–28], polyhydroxyalkanoates (PHAs) [10,11], and their mixtures [16,17]. Scaffolds composed of single polyesters can provide a reasonable three-dimensional (3D) space for cell adhesion, proliferation and migration, but they do not offer a desirable environment for osteogenic induction due to a lack of biologically functional substances [14].

Peer review under responsibility of KeAi Communications Co., Ltd.

* Corresponding author. Key Laboratory of Resource Biology and Biotechnology in Western China, Ministry of Education, School of Medicine, Department of Life Sciences and Medicine, Northwest University, Xi'an, 710069, China.

** Corresponding author. MOE Key Laboratory of Bioinformatics, Center for Synthetic and System Biology, School of Life Sciences, Tsinghua University, Beijing, 100084, China.

E-mail addresses: wuqiong@mail.tsinghua.edu.cn (Q. Wu), weidaixu@nwu.edu.cn (D.-X. Wei).

<https://doi.org/10.1016/j.bioactmat.2021.01.013>

Received 22 October 2020; Received in revised form 21 December 2020; Accepted 9 January 2021

2452-199X/© 2021 The Authors. Publishing services by Elsevier B.V. on behalf of KeAi Communications Co. Ltd. This is an open access article under the CC

BY-NC-ND license (<http://creativecommons.org/licenses/by-nc-nd/4.0/>).

In addition to calcium ions [7], bioactive osteogenic growth factors also offer an appropriate microenvironment for the adhesion and capture of stem cells or osteoblasts, leading to osteogenic differentiation both *in vitro* or *in vivo* [29–32]. Bone morphogenetic protein 2 (BMP2) is a typical protein-based growth factor, which is essential for osteogenic differentiation of stem cells or osteogenic precursor cells. BMP2 has powerful osteoinductive properties, and has accordingly been applied in bone regeneration to induce the differentiation of stem cells into osteoblast. To achieve this, a large number of delivery systems composed of different materials have been investigated for the sustainable release of BMP2 [33]. Related methods have been widely applied in orthopedics and bone regeneration research, in both animal models and clinical trials [33,34].

Phospholipids, main components of cell membranes, which often play a role of intermediary between the water phase and the oil phase

(organic phase) for applications in drug delivery field [25,32]. Due to the disadvantages of easy degradation, high cost and poor dispersion in polyesters, the use of untreated BMP2 in combination with polyesters was only reported in a limited number of studies [25,35]. In our previous study, we established soybean lecithin-mediated loading of nanoporous PLGA microspheres with large amounts of BMP2 for controlled release as a novel injectable stem cell carrier for *in-situ* osteogenesis *in vivo* [25]. Due to the introduction of soybean lecithin (SL) as a biosurfactant, the PLGA-based microspheres had a significantly higher BMP2 entrapment efficiency (EE) and controlled BMP2 release behavior, which resulted in excellent *in vitro* and *in vivo* stem cell proliferation, differentiation, and matrix mineralization. Traditional tissue engineering holds that cells must be seeded onto scaffolds prior to transplanting [10,11,14,16,17]. In other words, seeding and transplantation of exogenous cells pre-attached on scaffolds are the main

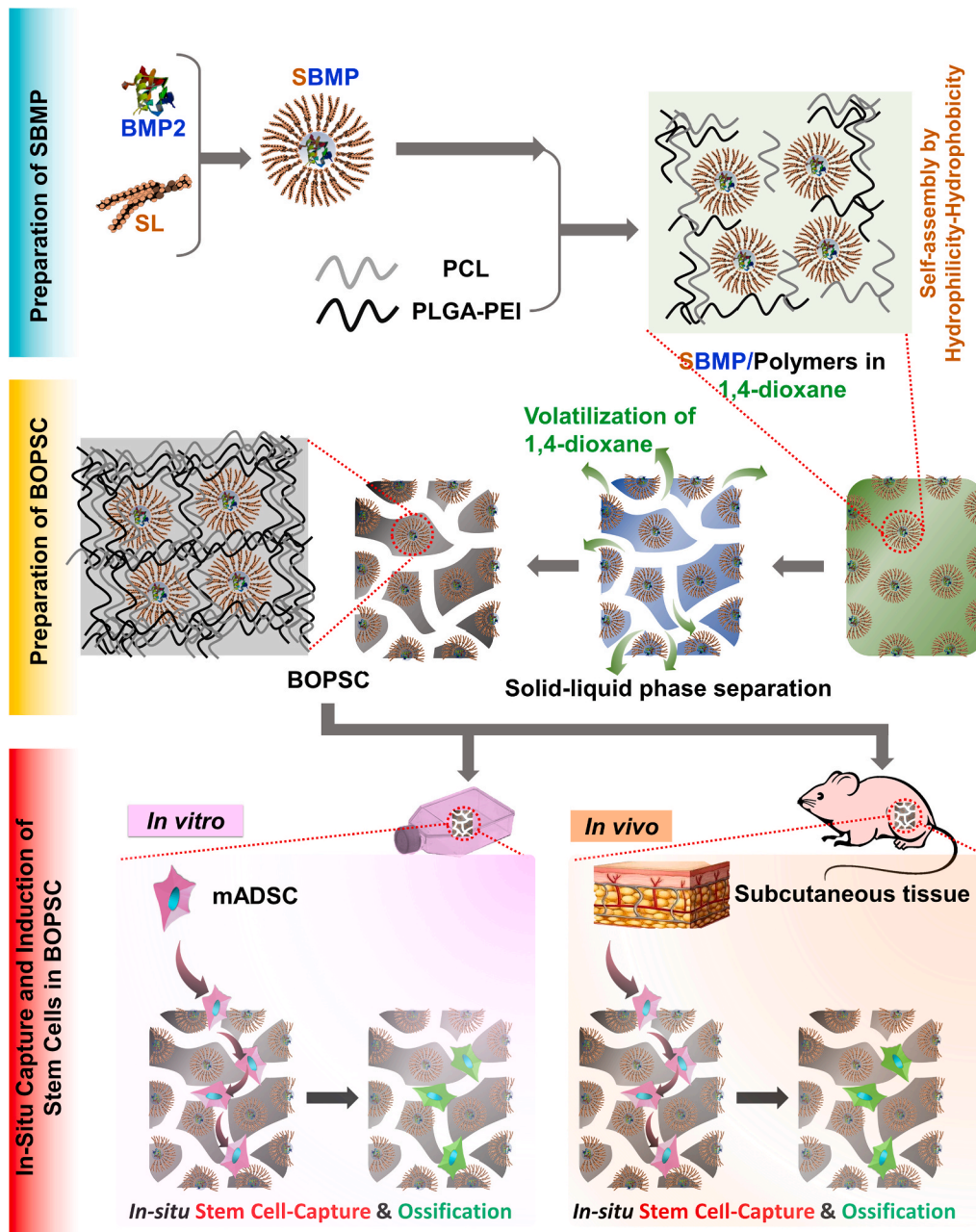


Fig. 1. Schematic of bioactive osteo-polyester scaffold (BOPSC) as a 3D cell-free platform for *in vitro* and *in vivo* stem cell capture and *in-situ* directed osteoinduction in bone tissue regeneration. SL: soybean lecithin; SBMP: SL-BMP2 complex; PLGA-PEI: Poly(lactide-co-glycolide)-co-polyetherimide; PCL: poly(ε-caprolactone); mADSC: mouse adipose derived mesenchymal stem cell.

approach. However, due to the change of microenvironment and related stress, death and function attenuation of exogenous cells often occur in transplants [10]. Consequently, it was also proposed in recent studies that the microstructure of cell-free scaffolds with embedded inducers can also promote cell migration or capture surrounding cells *in situ* [36–40].

Therefore, we exploited a soybean lecithin-mediated bioactive osteopolyester scaffold (BOPSC) composed of a combination of the PCL and poly(lactide-co-glycolide)-co-polyetherimide (PLGA-PEI) polyesters for repair of non-load-bearing bone (Schematic in Fig. 1), with high amounts of entrapped BMP2 for continuous release. These scaffolds were employed as a 3D cell-free platform for stem cell-capture and *in-situ* osteogenic induction, both *in vitro* and *in vivo*, demonstrating their great potential for applications in bone tissue engineering, especially repair of non-load-bearing bone.

2. Materials and methods

2.1. Reagents

Poly(lactide-co-glycolide)-co-polyetherimide (PLGA-PEI, $M_w = 10^5$ D, ratio of lactide: glycolide: etherimide = 49:50:1) and poly(ϵ -caprolactone) (PCL, $M_w = 10^4$ D) were purchased from Jinan Daigang Biomaterial Co., Ltd. (Shandong, China). Recombinant human bone morphogenetic protein 2 (BMP2) was purchased from R&D Systems (Minneapolis, MN, USA). Soybean lecithin (SL) containing 70%–97% phosphatidylcholine was purchased from Shanghai Taiwei Pharmaceutical Co. Ltd. (Shanghai, China). General reagents such as 1,4-dioxane were of analytical grade and were purchased from Sinopharm Chemical Reagent Co., Ltd. (Shanghai, China).

2.2. Preparation of SL-BMP2 complexes

The SL-BMP2 Complexes (SBMP) were prepared using a physical self-assembly method, as reported in our previous study [25]. Briefly, SL and BMP2 at a weight ratio of 5:1 were dissolved in dimethyl sulfoxide containing 5% (v/v) acetic acid by slow magnetic stirring at 30 °C for 24 h. Then, the complex was lyophilized for 12 h to remove the solvent. The lyophilized SBMP was hermetically sealed and stored at 4 °C until further use.

2.3. Determination of the solubility of SBMP

The solubility of SBMPs was determined by dissolving in ultrapure water or dichloromethane, as described previously [25]. Briefly, excess SBMPs were added to ultrapure water or dichloromethane in sealed glass containers. Then, the containers were gently shaken on an orbital shaker at 25 °C for 24 h. Subsequently, the samples were centrifuged at 6000 rpm for 10 min, and the resulting supernatant was removed for further analysis. To measure the solubility of SBMPs in ultrapure water, the BMP2 concentration was determined using a Quantikine human BMP2 ELISA kit (MERCK, Germany). To measure the solubility of SBMPs in dichloromethane, the dichloromethane in the collected supernatant was evaporated to obtain dry SBMPs, which were then dissolved in ultrapure water and measured as above. Six parallel measurements were performed for each sample.

2.4. Preparation of scaffolds loaded with BMP2

Scaffolds with SBMP (SBMP-SC group) were fabricated using a modified solid-liquid phase separation method [41]. Briefly, a series of PCL and PLGA-PEI mixed materials (weight ratio = 1:1) and 0.06 g SBMPs (containing 0.01 g BMP2) were dissolved in 5 ml 1,4-dioxane to form a homogeneous solution in 2 h. At a final concentration of BMP2 of 0.2 w/v%, the content of PCL/PLGA-PEI was 5 w/v%, 10 w/v% and 15 w/v%, respectively. The solution was poured into a cylindrical glass

mold of 10 ml, shock-frozen in liquid nitrogen, and then lyophilized for 1–2 days to form the resulting scaffolds. For control groups, scaffolds with BMP2 (named BMP-SC group) and pure scaffolds without BMP2 or SL/BMP2 (named SC group) were prepared according to the same procedure with or without BMP2, and different content of PCL/PLGA-PEI, respectively. All samples have been cut to discoid scaffolds with a diameter of 4 mm and thickness of 2 mm (≈ 10 mg) for follow-up experiments.

2.5. Preparation of section of the scaffolds

To observe the internal structure, the scaffolds were sectioned using a WEI Frozen Ordered Sectioning Method (WEI FOSM) developed in a previous study [10]. The WEI FOSM method allows more convenient and rapid sectioning of many samples in 4 steps compared with the liquid nitrogen frozen section method and cryostat microtome with embedded refrigerant, which produce irregular sections and require a time-consuming preparation process. Finally, the internal morphology of scaffolds was observed using a scanning electron microscopy (SEM, Quanta 200, FEI, Czech) at an accelerated voltage of 15 kV.

2.6. Characterization of scaffolds

To measure the water-absorbing capacity and interior space connectivity of various scaffolds, the water-uptake-ratio (WUR) was measured as described in previous studies [10,11]. After lyophilization for 12 h, the dried scaffolds were immersed in ultrapure water at room temperature for 72 h. Then, the excess water was removed using a filter paper. The water uptake rate of the scaffolds was calculated using the formula $WUR (\%) = (W_w - W_d) / W_d \times 100\%$, where W_w and W_d are the wet weight and dry weight of the scaffolds, respectively, and ($W_w - W_d$) is the weight of water taken up by the scaffolds. Each measurement was done with 4 parallel samples ($n = 4$).

To assess the internal space of various scaffolds, we measured the porosity as described in previous studies [10,11]. After lyophilization for 12 h, the dried scaffolds were immersed in absolute ethanol at room temperature for 10 min. The Porosity of the scaffolds was calculated using the formula $porosity (\%) = (V_0 - V_1) / (V_t - V_1) \times 100\%$, where V_0 is the initial volume of absolute ethanol added to the dried scaffolds, V_t is the total volume of the system when the scaffolds are immersed in the absolute ethanol, and V_1 is the volume of the residual liquid after the liquid-impregnated scaffolds are removed. Each measurement was done with 4 parallel samples ($n = 4$).

Element ratios of carbon (C), oxygen (O), nitrogen (N) and phosphorus (P) in the scaffolds were examined using an IE250X-Max50 Energy-dispersive X-Ray spectroscopy (EDS, Oxford Instruments, UK).

2.7. BMP2 entrapment efficiency of scaffolds

The BMP2 entrapment efficiencies (EEs) of different discal scaffolds were evaluated based on a published method [25]. Briefly, scaffolds were immersed in phosphate buffer saline (PBS) and stirred at 200 rpm and 4 °C for 30 s. The free BMP2 in the PBS supernatant, which was not packaged into scaffolds, was analyzed by using a Quantikine human BMP2 ELISA kit (MERCK, Germany). An equal amount of SBMP was dissolved in 100 ml PBS, and then subjected to the same procedure. After that, the active BMP2 contents were measured using the ELISA kit and the phospholipid assay kit, respectively. The entrapment efficiency was calculated using the formula $EE (\%) = (W_t - W_f) / W_t \times 100\%$ (3), where W_f and W_t are the content of collected free BMP2 and total amount of BMP2 during preparation, respectively. Four parallel measurements were performed for each sample ($n = 4$).

2.8. In vitro BMP2 release from scaffolds

To analyze the release of BMP2 as described before [7,25], scaffolds

of SBMP-SC group and BMP-SC group (≈ 10 mg) were immersed in 1 ml PBS in a 2 ml test tube and incubated on a shaker at 50 rpm and 37 °C for 30 days. The PBS was collected and replaced with a 500 μ l fresh release medium at the designated time points. The amount of released BMP2 in the collected PBS was determined using the Quantikine human BMP2 ELISA kit (MERCCK, Germany). Four parallel measurements were performed for each sample ($n = 4$).

2.9. *In vitro* biodegradation of scaffolds

Similarly to *in vitro* BMP2 release test, SBMP-SC group and BMP-SC group (≈ 10 mg) were immersed in 10 ml PBS in a 15 ml tube and incubated on a shaker at 50 rpm and 37 °C for 30 days. The residual scaffolds were air-dried at 25 °C in 6 h and weighted at the designated time points. And degradation rate of all dried scaffolds were calculated using the formula Degradation rate (%) = $(W_{res}/W_{tot}) \times 100\%$, where W_{res} and W_{tot} are the weight of residual and total scaffolds, respectively. Three parallel measurements were performed for each sample ($n = 3$).

2.10. Distribution of BMP2 in scaffolds

Based on our previous report [25], scaffolds were fixed with 4% paraformaldehyde for 30 min, permeabilized with 0.1% Triton X-100 (Invitrogen, USA) for 15 min, and then blocked with 3% bovine serum albumin (BSA; Sigma-Aldrich, USA) for 30 min. Then, scaffolds were incubated with primary antibody (rabbit anti-human BMP2, Invitrogen, USA) at 4 °C overnight and incubated in the specified secondary antibodies (Alexa488-conjugated rat anti-rabbit, Invitrogen, USA) for 1 h. Images were captured and analyzed with a confocal laser scanning microscopy (CLSM, Nikon, A1/N-SIM/N-STORM, Japan). The distribution of BMP2 on scaffolds surfaces was showed by a 3D reconstruction image from serial sections at the interval of 5 μ m. In order to analyze BMP2 distribution on the section of scaffolds, the sections of scaffolds were prepared by scalpel prior to the immunohistochemical staining process of BMP2. After staining, the section of scaffolds was imaged by CLSM at 488 nm. The distribution of BMP2 in middle section of scaffolds was also detected *via* same method.

2.11. Cultivation of stem cells

Mouse adipose derived mesenchymal stem cells (mADSCs) were obtained from Cyagen Biosciences (China), which were employed to study the cell capture, proliferation and differentiation as well as evaluate the biocompatibility of BOPSCs. The mADSCs cultured in mouse adipose-derived mesenchymal stem cell basal medium (BM, SYAGEN, China) in a humidified atmosphere comprising 5% carbon dioxide at 37 °C.

2.12. *In vitro* capture of stem cells and live/dead cell viability detection

To evaluate cell capture in only 12 h, 1×10^5 mADSCs were seeded onto sterilized discoid scaffolds with a diameter of 4 mm and thickness of 2 mm (≈ 10 mg) in 96-well tissue culture plate (TCP) coated with agarose and cultivated in BM for 12 h. The cell capture efficiency was calculated using the formula Cell capture efficiency (%) = $(N_{att}/N_{tot}) \times 100\%$, where N_{att} and N_{tot} are the numbers of cells attached to BOPSCs and on the TCPs, respectively. Six parallel measurements were performed for each sample ($n = 6$).

Using Live/Dead Cell Viability Kit (Invitrogen, USA), all scaffolds loaded with mADSCs were stained directly with calcein-AM (green colour) and ethidium homodimer-1 (red colour) for *in-situ* distribution observation of living and dead cells on scaffolds under CLSM at 488 nm and 561 nm.

2.13. *In vitro* proliferation and migration of stem cells in scaffolds

To evaluate cell proliferation, 1×10^5 mADSCs were seeded onto sterilized discoid scaffolds with a diameter of 4 mm and thickness of 2 mm (≈ 10 mg) in 96-well TCP coated with agarose and cultivated in BM for 1 day. Then, the scaffolds seeded with mADSCs were transferred to a new 48-well TCP with agarose coating and then cultivated in BM, for 7 days and 14 days, respectively. The culture medium was replaced with 1 ml of fresh BM daily. The viability of mADSCs on BOPSC was assessed using a CCK-8 assay kit (Dojindo, Japan) [11,25]. Briefly, at the designated time points, the culture medium was removed and 1 ml fresh BM containing 0.1 ml CCK-8 solution was added to each sample. The samples were then incubated at 37 °C for 2 h. All scaffolds with cells were immersed in DMEM (Gibco, USA). Aliquots comprising 200 μ l of the supernatant were transferred into a 96-well plate, and the absorbance was measured at 450 nm using a microplate reader (Multiskan MK3, Thermo Lab Systems, Finland). Six parallel measurements were performed for each sample ($n = 6$).

To assess the cell migration and distribution in different space, mADSCs in scaffolds were observed by CLSM and SEM, according to the previous method [10,11]. Briefly, scaffolds with cells were fixed using 4% paraformaldehyde in PBS for 20 min at room temperature. After washing three times with PBS, the scaffolds with mADSCs were immersed in 0.5% Triton X-100 solution (Invitrogen, USA) for 20 min and then washed 3 times with PBS. To stain actin and nuclei, the samples were incubated with Phalloidin-Alexa555 (red colour) (Invitrogen, USA) for 25 min and then with DAPI (Invitrogen, USA) for 5 min at room temperature. For observation of distribution in inner space, the scaffolds were cut *via* WEI Frozen Ordered Sectioning Method (WEI FOSM), after above treatments. Finally, the stained cells on scaffolds were observed under a confocal laser scanning microscopy (CLSM, Nikon, A1/N-SIM/N-STORM, Japan) with an excitation wavelength of 405 nm and emission wavelength of 561 nm.

For SEM observations, scaffolds with cells were fixed with 5% glutaraldehyde for 12 h and then dehydrated in a graded series of ethanol solutions comprising 30 vol%, 50 vol%, 60 vol%, 70 vol%, 80 vol%, 90 vol%, 95 vol% and 100 vol%, each for 15 min. The dehydrated samples were subsequently freeze-dried overnight to remove residual ethanol and observed under a SEM at 15 kV. For section, the scaffolds were sectioned using a WEI FOSM, after above treatments.

2.14. *In vitro* osteogenic differentiation ability of mADSCs on BOPSCs

To assess the osteogenic differentiation of mADSCs cultured on sterilized discoid scaffolds, Alkaline phosphatase (ALP) expression was analyzed. Briefly, after 1, 7 and 14 days of culture on scaffolds, the culture medium was removed and the scaffolds were washed 3 times with PBS to avoid interference from the remaining medium. 200 μ l 0.1% Triton X-100 was added and incubated for 10 min. Then, the supernatants were collected, to measure the ALP activity and total protein content using ALP activity kit (Shanghai Fusheng Biotechnology Development Co., Ltd, Shanghai, China), and protein assay kit (Tiangen, Beijing, China), respectively, according to the manufacturer's instructions. Three parallel measurements were performed for each sample ($n = 3$).

To investigate differentiation and matrix mineralization of mADSCs on scaffolds, the expression levels of osteogenic genes at 14 days after seeding were estimated by qRT-PCR analysis, as described in a previous study [25]. Briefly, the QuantiTect SYBR Green PCR kit (Qiagen, Hilden, Germany) was used to measure the levels of six markers in bone repair, including runt-related transcription factor 2 (Runx2), osteopontin (OPN), collagen-type I (COL-1), osteocalcin (OCN) and bone sialoprotein (BSP). Glyceraldehyde 3-phosphate dehydrogenase (GAPDH) was used as an internal reference gene. The sequences of the primers are shown in Table 1. According to the instruction of the PCR Kit, total RNA of cells for each scaffold was purified to synthesize the complementary

Table 1
Primer sequences used for gene expression analysis by qRT-PCR in this study.

Marker Gene	Primer sequences	
	Forward	Reversed
Runx2	TTCTCCAACCCACGAATGCAC	CAGGTACGTGTGGTAGTGAGT
OCN	TCTGATGAGACCGTCACTGC	AGGTCTCATCTGTGGCATC
BSP	GAATCCACATGCTATTGC	AGAACCCACTGACCCATT
Col I	CCCAGAGTGAACAGCGATT	ATGAGTTCTTCGCTGGGGTG
OPN	ACCAAAGTGAATGCCGAGAG	TCTGTGGTGAGGTTTCGAGTG
GAPDH	GACTTCAACAGCAACTCCAC	TCCACCACCTGTTGCTGTA

Runx2: runt-related transcription factor 2; OCN: osteocalcin; BSP: bone sialoprotein; COLI: collagen type-1; OPN: osteopontin; and GAPDH: glyceraldehyde 3-phosphate dehydrogenase.

DNA (cDNA). Three parallel measurements were performed for each sample.

2.15. Implantation of BOPSCs, *in vivo* capture of cells and *in situ* osteoinduction

Sterilized discoid scaffolds with a diameter of 4 mm and thickness of 2 mm (≈ 10 mg) were implanted subcutaneously on the back of 6-week-old C57BL/6 male mice (five mice per group). The implanted scaffolds were harvested after 6 months and fixed in 4% paraformaldehyde for further analysis. All mice were housed in isolated ventilated cages (maxima six mice per cage) in the animal facility of Tsinghua University. The mice were maintained on a 12/12-hour light/dark cycle, at 22–26 °C with sterile pellet food and water *ad libitum*. The laboratory animal facility was accredited by AAALAC (Association for Assessment and Accreditation of Laboratory Animal Care International), and the IACUC (Institutional Animal Care and Use Committee) of Tsinghua University approved all animal protocols used in this study.

To describe the migration ability of cells grown into internal space of scaffolds after cell-capture in subcutaneous tissues, we defined a migration distance (MD), based on observation of H&E staining sections of scaffolds in 4 weeks. As shown in Fig. 7a, MD is the length of black line (= 0 μm) and red line. The black lines indicate general interface of subcutaneous tissue and scaffolds; and the red lines indicate general interface of captured cells in scaffolds and blank space of scaffolds.

2.16. H&E staining, masson's trichrome staining, and immunohistochemical analysis of OCN

The implanted scaffolds with surrounding tissue were removed, fixed with paraformaldehyde, and decalcified in 10 w/v% ethylenediaminetetraacetic acid (pH = 7.4) for 1–2 weeks, followed by dehydration and paraffin embedding. Sections were cut for H&E staining and Masson's trichrome staining using the Trichrome Stain (Masson) kit (Thermo Fisher Scientific, USA), as described previously [23]. OCN expression was evaluated by immunohistochemical analysis, as described previously [15]. The sections were blocked with 3% BSA for 30 min and then incubated with a primary antibody against OCN (Thermo Fisher Scientific, USA) at 4 °C overnight, followed by a secondary antibody (Thermo Fisher Scientific, USA). Finally, the sections were observed under an optical microscope (IX83, Olympus, Japan).

2.17. Micro-CT analysis

Micro-CT analysis of implanted scaffolds was performed using a Quantum GX micro-CT system (PerkinElmer, USA). The X-ray source was set at a node current of 500 mA and 80 kV, with an exposure time of 4 min for each of the 360° rotational steps. Image slices were then reconstructed using micro-CT image analysis software (Inveon Research Workplace). The 3D reconstruction and volume quantification of the implant-derived ectopic bone was performed using standardized

thresholds. The region of interest was selected, and the lower and upper threshold values for bone were set. The bone mineral density (BMD, mg cc^{-1}) and ratios of new bone volume to existing tissue volume (BV/TV, %) were calculated by the software.

2.18. Statistical analysis

All data were expressed as means \pm standard deviations of the indicated number of parallel experiments. Statistical comparisons were made using Student's *t*-test. Differences with *p*-values <0.05 were considered statistically significant.

3. Results and discussion

3.1. Morphology and characters of scaffolds

In our earlier reports [25,32], we developed a physical mixture method for soybean lecithin-mediated introduction of growth factors into polyesters (SMIGP method), in which hydrophilic BMP2 was firstly modified by blending with the biosurfactant soybean lecithin (SL) to form hydrophobic SL-BMP2 complexes, named SBMP. Then solid-liquid phase separation was used to prepare the bioactive osteo-polyester scaffold (BOPSC) of PCL and PLGA-PEI with SBMP for *in situ* cell-capture and osteogenic induction of stem cells (Fig. 1).

In this study, soybean lecithin-mediated BMP2 polyester scaffolds (BOPSCs) are white appearance, which was defined as SBMP-SC group (Fig. 2a). As controls, polyester scaffolds with only BMP2 or nothing were produced *via* analogous methods, and were named BMP2 polyester scaffolds (BMP-SC group) and pure polyester scaffolds (SC group), respectively (appearance and schematic in Fig. 2a). The polyester content of 50% PCL blended with 50% PLGA-PEI in 1,4-dioxane was 5 w/v %, 10 w/v% and 15 w/v%, respectively, were named SBMP-5SC, SBMP-10SC and SBMP-15SC for SBMP-SC group; BMP-5SC, BMP-10SC and BMP-15SC for BMP-SC group; and 5SC, 10SC and 15SC for SC group, respectively.

After freeze-drying, the morphology of polymer scaffolds was analyzed by SEM. As shown in Figs. 2a and 2b, the morphology of all polyester scaffolds with 10 w/v% and 15 w/v% of polyester had a more regular porous structure. However, polyester scaffolds produced using 5 w/v% of polyester content had an irregular structure in all groups. Low concentration of polyester may lead to structure collapse *via* solid-liquid phase separation, which was described in previous study [43].

Generally, these scaffolds have an appropriate porous structure and microenvironment that promotes adhesion and growth of cells, simulating the microstructure and function of natural bone. Too large structures are not conducive to cell adhesion, leading to a low cell adherence rate *in vitro* [13,14]. Conversely, too small pores can limit cell proliferation, metabolism and even differentiation [11]. With the increase of the polyester content in the organic solvent, the mean pore size of scaffolds decreased from 50–80 μm to 20–50 μm . Therefore, it is necessary to adjust the concentration of biomaterials in organic solvents to obtain an appropriate microstructure and internal space of polyester scaffolds, as has been widely reported in previous studies [41]. The range of inner pore sizes of SBMP-5SC and BMP-5SC was greater than in the other preparations. However, introduction of BMP2 or SL with the same polyester content of 10 w/v% did not significantly disturb the pore size of the polyester scaffolds (Fig. 2c). Similar to our previous reports [25,32], the properties of polyester microspheres and nanoparticles was also not changed by complexes of SL and BMP2, including size, surface charge and microstructure.

As expected, the SBMP-SC group had a high BMP2 entrapment efficiency (EE) of 94.6%–97.5%, because SL increased the solubility of BMP2 while also protecting it in the organic phase (Table 2). By contrast, the EE of the BMP-SC group was only 33.2%–36.5%, approximately 1/3 of the SBMP-SC group. Similar soybean lecithin-mediated PLGA microspheres with high BMP2 entrapment efficiency were

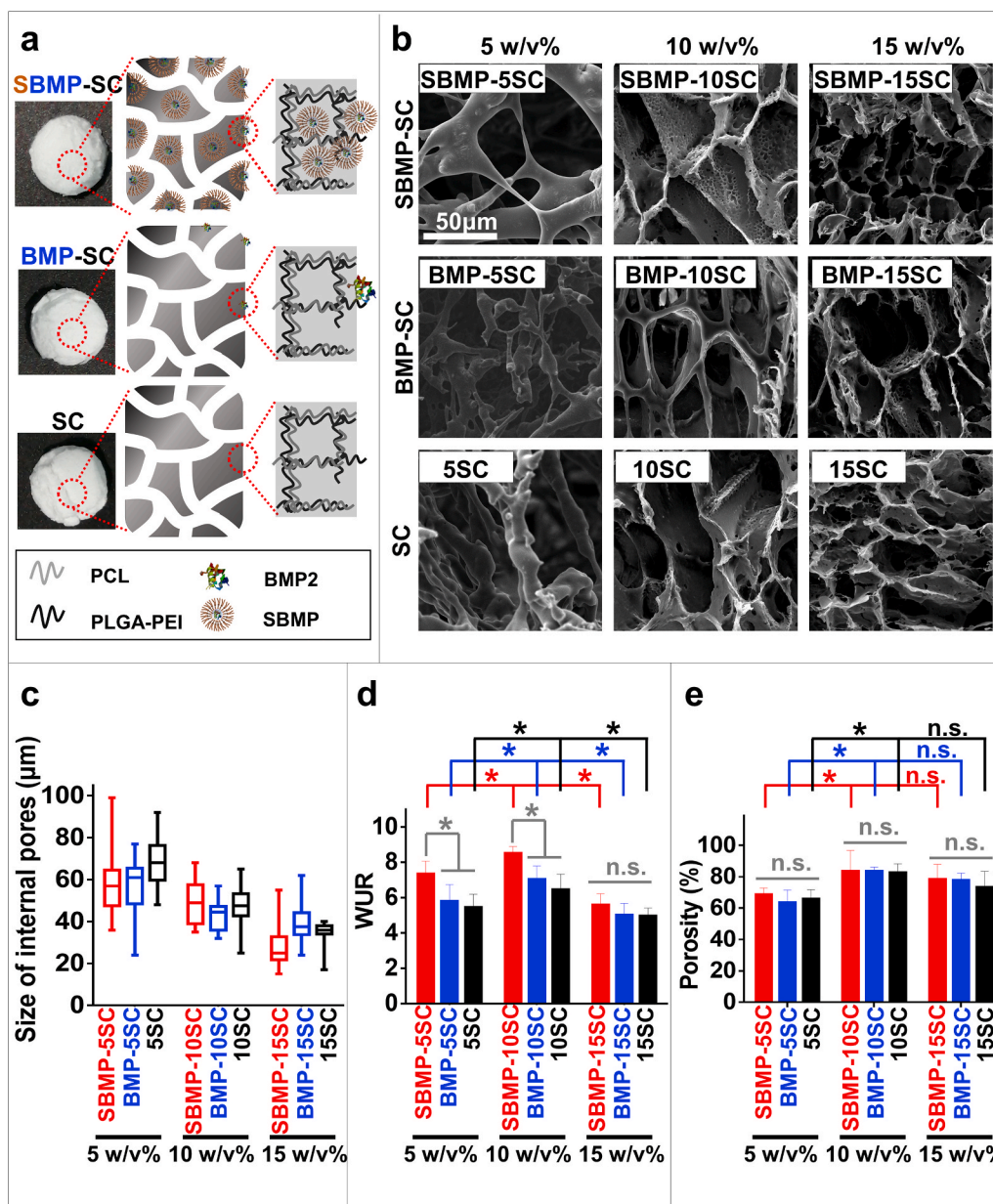


Fig. 2. Characteristic and morphology of various scaffolds. a) Micro-structure schematic of the SBMP-SC with SBMPs (SBMP-SC group), BMP-SC with pure BMP2 (BMP-SC group) and SC scaffolds (SC group). b) SEM images, c) size of internal pores, d) water uptake ratio (WUR), and e) porosity of various scaffolds. A total of size in (c) was measured in random 25 internal pores in (b); and four parallel measurements were evaluated in (d) and (e), * $p < 0.05$, n.s. = no significant difference.

Table 2
Elemental composition of scaffolds according to analysis of EDS spectra.

Samples	Mean EE (%)	The ratio of elements (%)				
		C	O	N	P	Others
SBMP-5SC	94.58	40.443	54.414	1.111	4.011	0.021
SBMP-10SC	95.35	38.125	50.633	2.021	9.210	0.012
SBMP-15SC	97.45	38.247	46.087	2.131	13.522	0.014
BMP-5SC	33.22	44.112	55.551	0.321	0.000	0.017
BMP-10SC	33.97	54.714	44.905	0.368	0.000	0.013
BMP-15SC	36.49	54.343	45.243	0.387	0.012	0.015
5SC	–	44.207	55.790	0.001	0.002	0.000
10SC	–	45.009	54.989	0.002	0.000	0.000
15SC	–	44.862	55.118	0.004	0.001	0.015

reported in our previous study [25].

Due to excellent biosafety and effectiveness, SL, a small amphipathic molecule, has been widely explored as surfactant for oil-in-water emulsions in pharmaceutical preparation. In SBMP, SL can play a role of surfactant to coverage BMP2 with its hydrophilic segment, and its opposite hydrophobic segment expose to the outside for resisting to organic solvent. It can improve dispersion capacity of BMP2 and protect BMP2 in polymer/1,4-dioxane solution, due to amphipathy.

Subsequently, EDS spectra of the polyester scaffolds were analyzed. As shown in Table 2, SBMP-SC group showed the presence of significant amounts of nitrogen (1.111%–2.131%), more than BMP-SC group (0.321%–0.387%) or SC group (0.001%–0.004%). By contrast, phosphorus was only found in SBMP-SC group (4.011%–13.522%). These results suggest that the SBMP were successfully blended into the SBMP-SC group using the SMIGP method. Conversely, only low amounts of BMP2 were incorporated into BMP-SC without SL. Moreover, the

percentage of P and N in SBMP-SC group both presented a rising tendency with the increase of polyester content in the organic solvent, which indicated that the polyester proportion could retain more SBMP.

Tissue engineering usually requires scaffolds with a high porosity and reasonable hydrophilicity to provide sufficient internal space for cell capture and growth [42–44]. Consequently, porosity is an important criterion for estimating a scaffold design. After the introduction of BMP2 or SL and optimal polyester content, the SBMP-10SCs showed a highest water uptake ratio (WUR) of 850%, more than all other preparations (Fig. 2d). This high WUR was explained in previous research [25].

Moreover, the SBMP-5SC, SBMP-10SC and SBMP-15SC showed high porosities of 83.4%, 83.3% and 82.6%, respectively, which was similar to other preparations with the same polyester content (Fig. 2e). Therefore, the blending BMP2 and SL into the polyesters did not change the porosity of the polyester scaffolds, but increased their WUR.

3.2. In vitro BMP2 release and biodegradation of scaffolds

The *in vitro* BMP2 release and biodegradation behaviors of the SBMP-SC group and BMP-SC group were analyzed, and the cumulative released rate curves and released amount of BMP2 are both shown in Fig. 3a and b. The SBMP-SC group showed a clear initial burst release phase, with 15%–35% (≈ 110 ng/ml BMP2 content) of cumulative release in the first day, followed by a slow-release phase driven by the biodegradation of the polyesters, with 53.5%–71.0% release from day 2 to day 30. This is a typical biphasic behavior for BMP2 release, which provided a sustained BMP2 supply for osteogenic differentiation of stem cells on SBMP-SC group, as a previous report for BMP2 release behavior from soybean lecithin-mediated nanoporous PLGA microspheres demonstrated [25]. Moreover, the SBMP-10SCs showed optimal cumulative amount of released BMP2 (≈ 178 ng/ml) in SBMP-SC group, and was 8-fold of that of BMP-SC group (≈ 22 ng/ml).

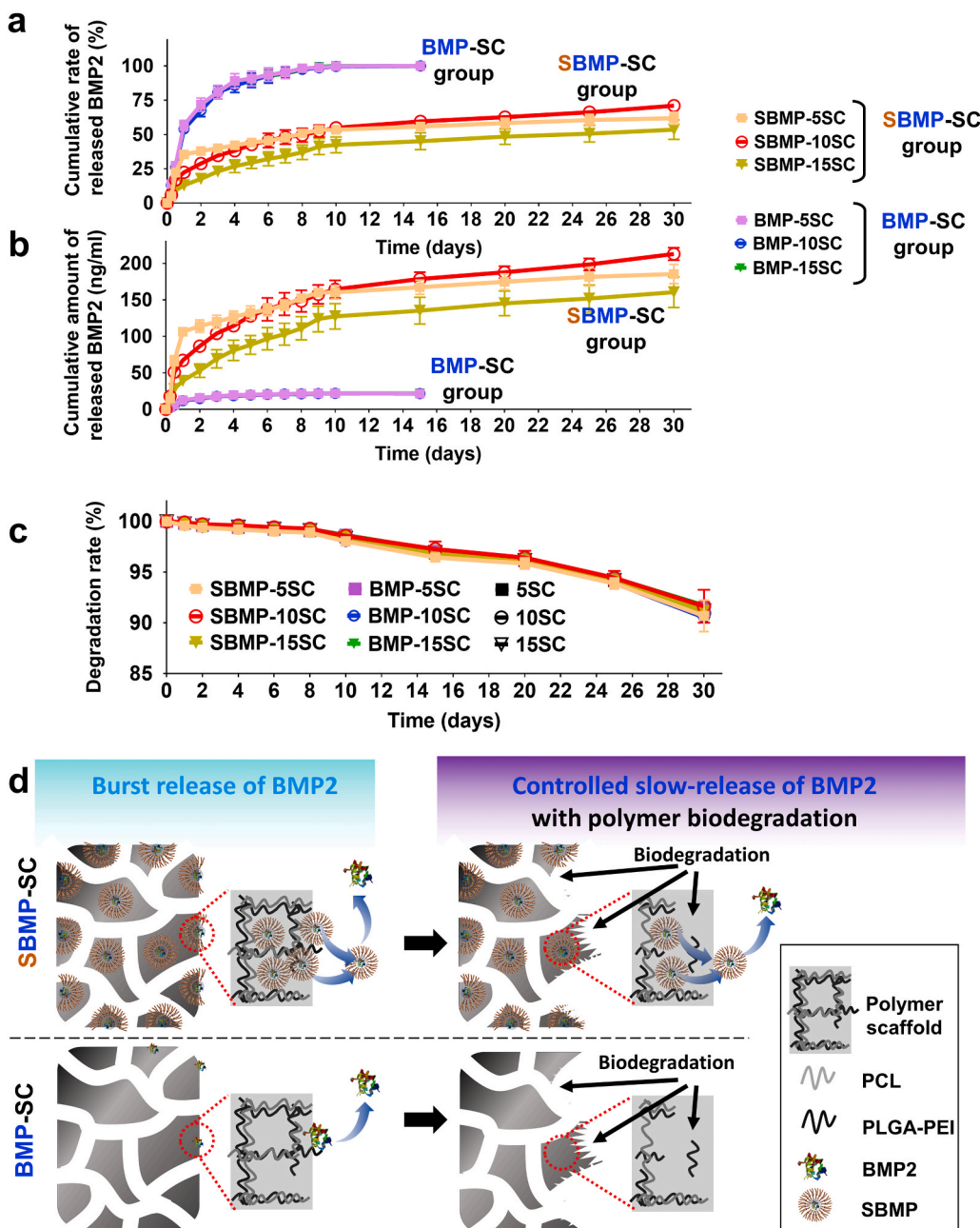


Fig. 3. Comparison of *in vitro* BMP2 release and biodegradation behaviors of various scaffolds in PBS (pH = 7.4) supplemented with 0.1% BSA at 37 °C for 30 days. a) *In vitro* cumulative release rate of BMP2 (%) and b) cumulative amount of released BMP2 (ng/ml) of SBMP-SC Group and BMP-SC Group in 30 days. n = 3. c) Biodegradation rate of SBMP-SC group, BMP-SC group and SC group, respectively. d) Schematic of *in vitro* controlled slow-release of BMP2 from SBMP-SC with polymer biodegradation, comparison with BMP-SC group.

In Fig. 3a and b, the control BMP-SC group without SL also presented a fast burst release in the first days, with 54%–55% of cumulative release rate and few effective BMP2 (≈ 3.1 ng/ml). Up to 100% (≈ 21.5 ng/ml) on day 9, released BMP2 of the BMP-SC could not provide a long-term signal to effectively facilitate osteogenic differentiation of stem cells *via* degradation of the polyesters. The difference of cumulative BMP2 release among BMP-5SC, BMP-10SC and BMP-15SC was negligible.

Similarly, in pre-reports [27], initial burst release of BMP2 from SBMP-SC and BMP-SC groups was mainly resulted by unstable BMP2-loading on surface of scaffolds. However, continuous polymer-degradation promoted a long-term effective supply of BMP2 from SBMP-SC group, as shown in Fig. 3d. Interestingly, all scaffolds remain a slow degradation and have a similar degradation rate of 90%–91% on day 30 (Fig. 3c), which explained microstructure and introduction of SL or BMP2, cannot change degradation.

Therefore, due to suitable microstructure, highest WUR and porosity, and perfect BMP2-supply with slow biodegradation, the SBMP-10SC was the best candidate of bioactive cell-free-scaffolds, which was defined as bioactive osteo-polyester scaffolds (BOPSCs) for in-vitro/in-vivo capture

and directed osteo-induction. And BMP-10SC and 10SC were controls.

3.3. Distribution of BMP2 in BOPSCs

To investigate the distribution of BMP2 in different spaces, we defined two areas of BOPSCs: surface and section as shown in Fig. 4a and b; and activated BMP2 on BOPSCs were immunohistochemically stained using an antibody against BMP2. In Fig. 4c, abundant green fluorescence fixed on both surface and section of BOPSCs, but few on surface of BMP-10SCs and noting for others, which demonstrate that only BMP2 modified by SL can be distributed into whole scaffold.

3.4. In vitro capture, proliferation and migration of mADSCs in BOPSCs

Ideal tissue engineered scaffolds can realize capture, proliferation and migration of cells over a longer period. Compared with the pure polymer scaffolds (10SCs), BOPSCs and BMP-10SCs showed a higher cell capture efficiency of 80%, most likely due to the presence of SL or BMP2 in PCL/PLGA-PEI (Fig. 4d). Hence, with the introduction of BMP2, the

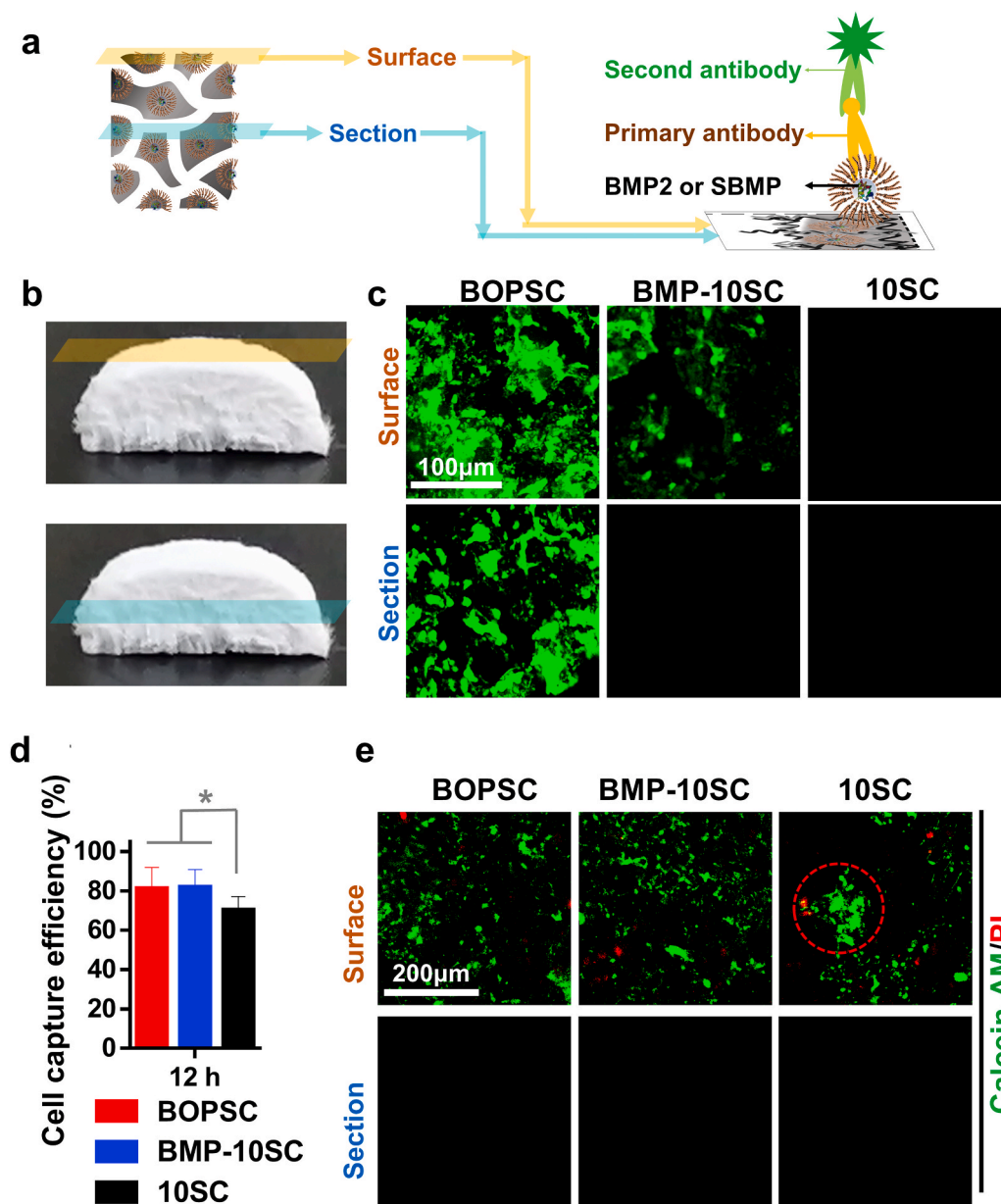


Fig. 4. Distribution of BMP2 and cell-capture of BOPSCs and control scaffolds. a) Schematic of immunohistochemical staining of BMP2 on BOPSCs. b) Photograph of BOPSC with surface and section. c) CLSM observation of BMP2 distribution on the surface and section of BOPSCs and controls. d) Cell capture efficiency of mADSCs on surface of BOPSCs and control scaffolds after only 12 h of seeding. Six parallel measurements in (d), $**p < 0.01$. e) CLSM observation of living and dead mADSCs on BOPSCs, BMP-10SCs and 10SCs after 12 h. The red ring indicates aggregations of mADSCs on 10SCs.

cells capture efficiency of mADSCs on the polyester scaffold increased, which suggest that the loaded and released BMP2 molecules retained good bioactivity and were also able to assist the capture of cells dissociated in medium to PCL/PLGA-PEI. In previous reports [25,32], carriers composed of other polyester materials for the loading and release of BMP2, such as 2D films or 3D scaffolds/microspheres, were also found to promote the attachment of stem cells on surface, similar to our results.

In addition, superior design of the microstructure and material properties can promote cell growth and metabolic function. Hence, the capture of cells dissociative in BM can be changed by adjusting the hydrophobicity or other interfacial characteristics of biomaterials. As expected, all scaffolds were able to capture mADSCs in only 12 h. However, more living mADSCs labeled by calcein-AM (green color) and less dead mADSCs labeled by ethidium homodimer-1 (red color) were found on surface of BOPSC and BMP-10SCs (Fig. 4e). Furthermore, some cell aggregations emerged on 10SCs, which was different from the uniform cell distribution on BOPSCs and BMP-10SCs. However, no any

living or dead cells were found in sections of all scaffolds, which also explained mADSCs cannot migrate to inner of spongy scaffolds in only 12 h in this study, even with assisting of BMP2.

The *in vitro* proliferation and migration of mADSCs continuously grown in different space of scaffolds was evaluated after 1, 7, and 14 days (Fig. 5a). As shown in Fig. 5b, the cell viability of BOPSCs and BMP-10SCs was better than that of the control 10SCs on day 1 and day 7 ($p < 0.05$), which was similar to the results of cell capture. However, on day 14, BOPSCs still showed the best cell viability, and BMP-10SCs had similar cell viability to 10SCs. In some previous reports, proteins were found to promote cell growth during 7–15 days or in longer time due to effective parts or functional peptides of proteins, such as RGDs [45,46], collagen [47–49], gelatin [50–52], or silk fibroin [53]. As an important protein associated with osteogenesis, BMP2 had a similar effect in terms of proliferation and ossification [7]. In addition to scaffolds, BMP7-loaded nano-scale polyester particles or BMP2-loaded micro-scale polyester spheres also affected the cell activity and osteogenesis of

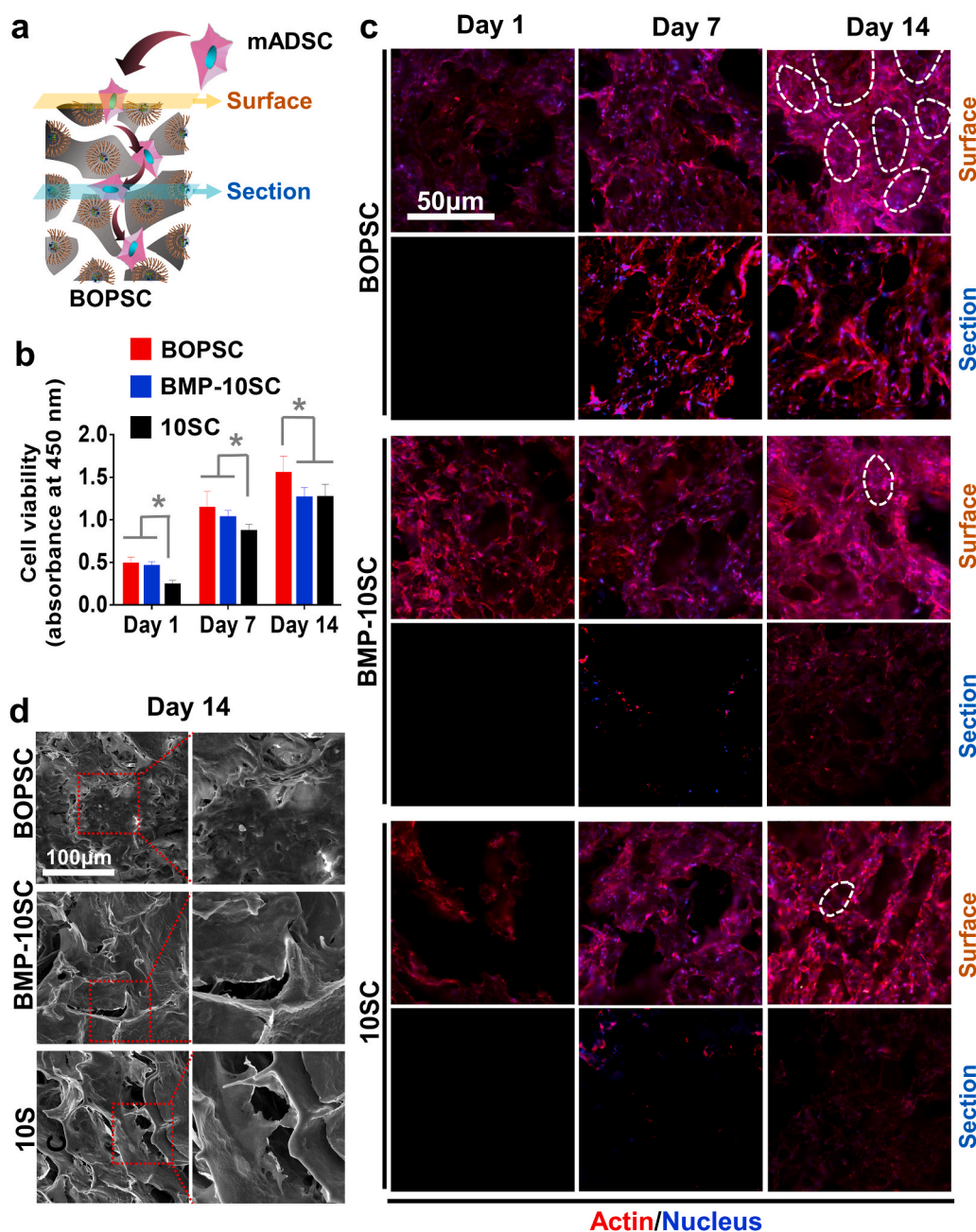


Fig. 5. Proliferation and migration of mADSCs in BOPSCs and control scaffolds. a) Schematic of capture, proliferation and migration of mADSCs in BOPSCs. b) Cell viability of mADSCs on BOPSCs, BMP-10SCs and 10SCs, respectively, in 14 days. Six parallel measurements in (b), $*p < 0.05$. c) CLSM images of mADSCs on surface and section of BOPSCs, BMP-10SCs and 10SCs in 14 days. The white rings indicate mADSCs adhering on inner space of pores in BOPSCs and controls in (c), respectively. d) SEM observation of mADSCs on BOPSCs, BMP-10SCs and 10SCs after 14 days.

bone-marrow mesenchymal stem cells [25,32].

As shown in Fig. 5c, mADSCs colored with Phalloidin-Alexa555 (red) and DAPI (blue) growing on the porous microstructure of the scaffolds. In all groups, the amount of cells on surface of scaffolds increased from day 1 to day 14. More mADSCs adhered to inner space of pores (indicated by white rings in Fig. 5c), comparison with controls. Due to cell-proliferation and insufficient growth space, mADSCs chose to downward migration into inner of scaffolds [10]. Comparison with BMP-10SCs and 10SCs, more mADSCs continuously migrated into inner of BOPSCs for 14 day, as evidenced by increasing fluorescence of stained cells in sections of BOPSCs.

By SEM, morphology of mADSCs attached to the inner space of pores on surface of BOPSCs (Fig. 5d), similar to the results of CLSM (Fig. 5c). Thus, the self-assembly of BMP2 into the polyester appears to have led to sustained cell-capture in BOPSCs over a longer period, which could

promote directional differentiation and tissue regeneration with more active stem cells growth.

3.5. In vitro osteogenic induction of mADSCs on BOPSCs

In bone tissue engineering and bone regeneration, BMP2 has been demonstrated to be effective for osteogenic differentiation of stem cells. Thus, we further compared the *in-situ* osteogenic differentiation capacity of BOPSCs and controls after 14 days of incubation (Fig. 6a). As shown in Fig. 6b, osteocalcin (OCN), a typical late osteogenic differentiation marker, was expressed in mADSCs on BOPSCs at high levels on day 14, significantly more than on other scaffolds. ALP activity of mADSCs on BOPSCs was also greatly increased compared with BMP-10SC and 10SC, reaching up to 9.839 U/mg protein (Fig. 6c). On day 1, ALP activity of BMP-10SCs (3354 U/mg protein) was similar to that of BOPSCs (4.210

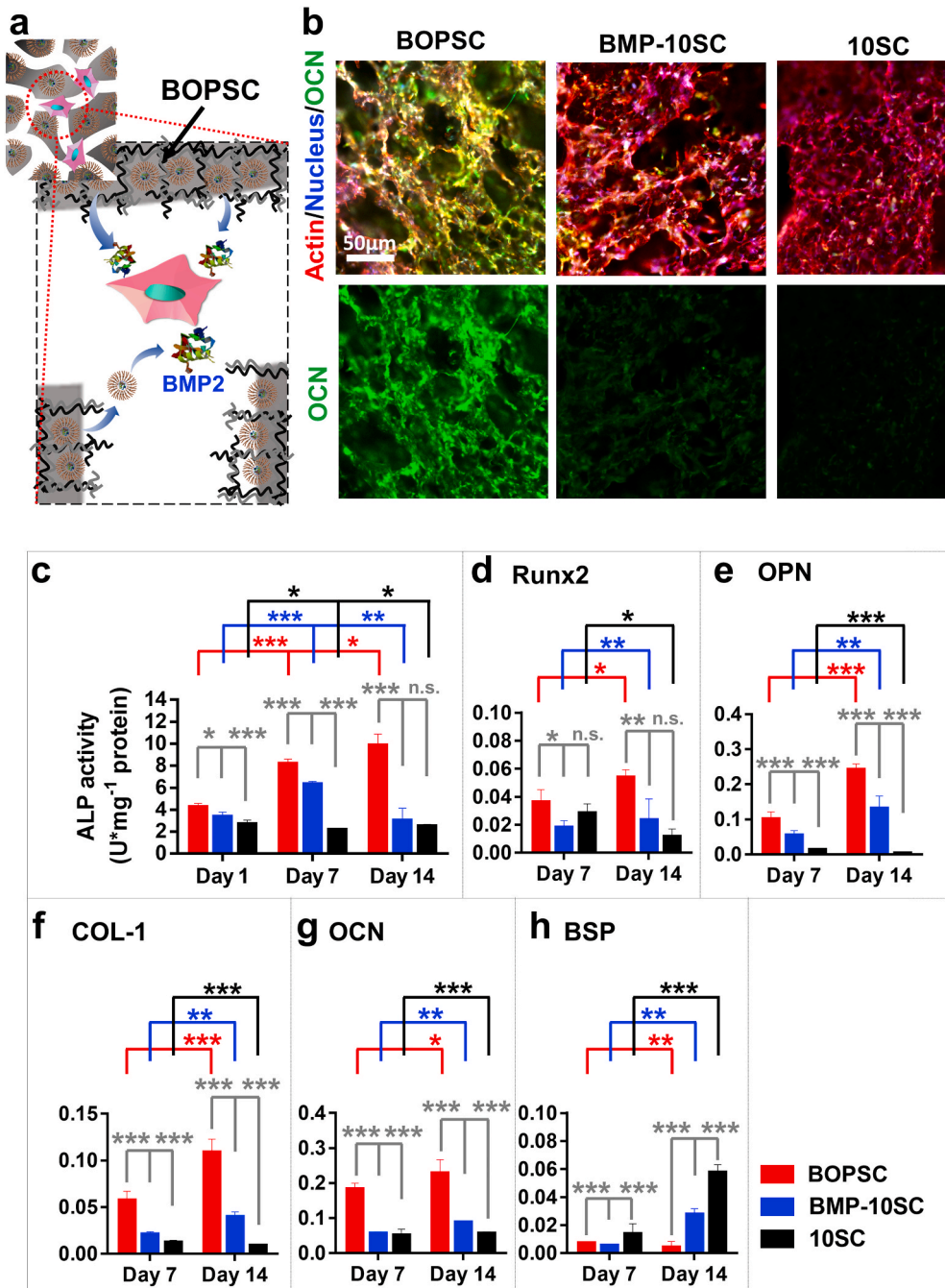


Fig. 6. *In vitro* osteogenic differentiation assays of BOPSCs and control scaffolds. a) Microenvironment schematic of *in-situ* osteogenic induction of mADSCs in interior pore of BOPSCs with BMP2-release. b) CLSM observation of OCN expression and distribution of mADSCs in BOPSCs and control scaffolds at day 15. c) ALP activity assay of mADSCs cultured on BOPSCs and control scaffolds. ALP activity was determined as enzyme activity units (U) per milligram of protein. d-h), Quantitative PCR analysis of osteogenic gene marker expression in mADSCs cultured on BOPSCs and control scaffolds after 7 and 14 days, respectively, including d) runt-related transcription factor 2 (Runx2), e) osteopontin (OPN), f) collagen-type I (COL-1), g) osteocalcin (OCN), and h) bone sialoprotein (BSP). The Y-axis represents the relative expression ($2^{-\Delta CT}$) normalized to the expression level of the housekeeping gene GAPDH. Statistically significant difference in c)-h), *p < 0.05, **p < 0.01, ***p < 0.005, n.s. = no significant difference, n = 3.

U/mg protein). However, the ALP activity of BMP-10SCs increased to 6.294 U/mg protein on day 7 and decreased to 2.978 U/mg protein on day 14. As a control, 10SCs without any BMP2 did not show any increase.

Furthermore, five biomarkers of bone repair were analyzed on day 7 and day 14. Four genes, runt-related transcription factor 2 (Runx2), osteopontin (OPN), collagen-type I (COL-1) and osteocalcin (OCN), all showed a positive tendency on BOPSCs, and were expressed at markedly higher levels than on BMP-10SC or SC on day 7 and day 14 (Figs 6d-g). At the same time, bone sialoprotein (BSP), a calcification inhibitor, was sustainably downregulated in cells on BOPSCs and the final expression level was down to only 15.4% of that on BMP-10SCs and 7.3% of that on SC (Fig. 6h). Thus, the ALP activity, OCN expression, and gene expression analysis confirmed that BOPSCs had better *in vitro* cell differentiation promoting effect on mADSCs than the other scaffolds. It should be noted that PCL/PLGA-PEI scaffolds with sustaining BMP2 release had the best promoting effect on the *in vitro* differentiation of stem cells. Continuous BMP2 supply, whether free or from polyester loading, can upregulate the expression levels of molecular markers related to the

bone differentiation, such as Runx2 [54,55], OPN [56,57], COL-1 [58] and OCN [59], as well as simultaneously downregulate the expression of BSP [60].

3.6. *In vivo* cell-capture on BOPSCs and osteogenic induction for bone reconstruction

In traditional tissue engineering, cells should be seeded in/onto biomaterials (scaffolds or carriers) and co-cultured *in vitro*. After healthy growth of the cells in/on the carrier, the carrier with pre-grown cells is implanted for *in vivo* evaluation. In our design, BOPSCs are implanted as cell-free-scaffolds, with the aim of capturing stem cells and stimulating ossification *in situ*, avoiding the seeding of exogenous cells and *in vitro* co-culture (Fig. 7a). To evaluate the *in vivo* capture of cells in subcutaneous tissue, osteogenic induction and potential repair for non-load-bearing bones, BOPSCs and controls (BMP-10SCs and 10SCs) were implanted into subcutaneous tissues of C57BL/6 mice for 6 months of proliferation and reconstruction. Based on observation of H&E staining sections of BOPSCs, BMP-10SCs and 10SCs, we defined a migration

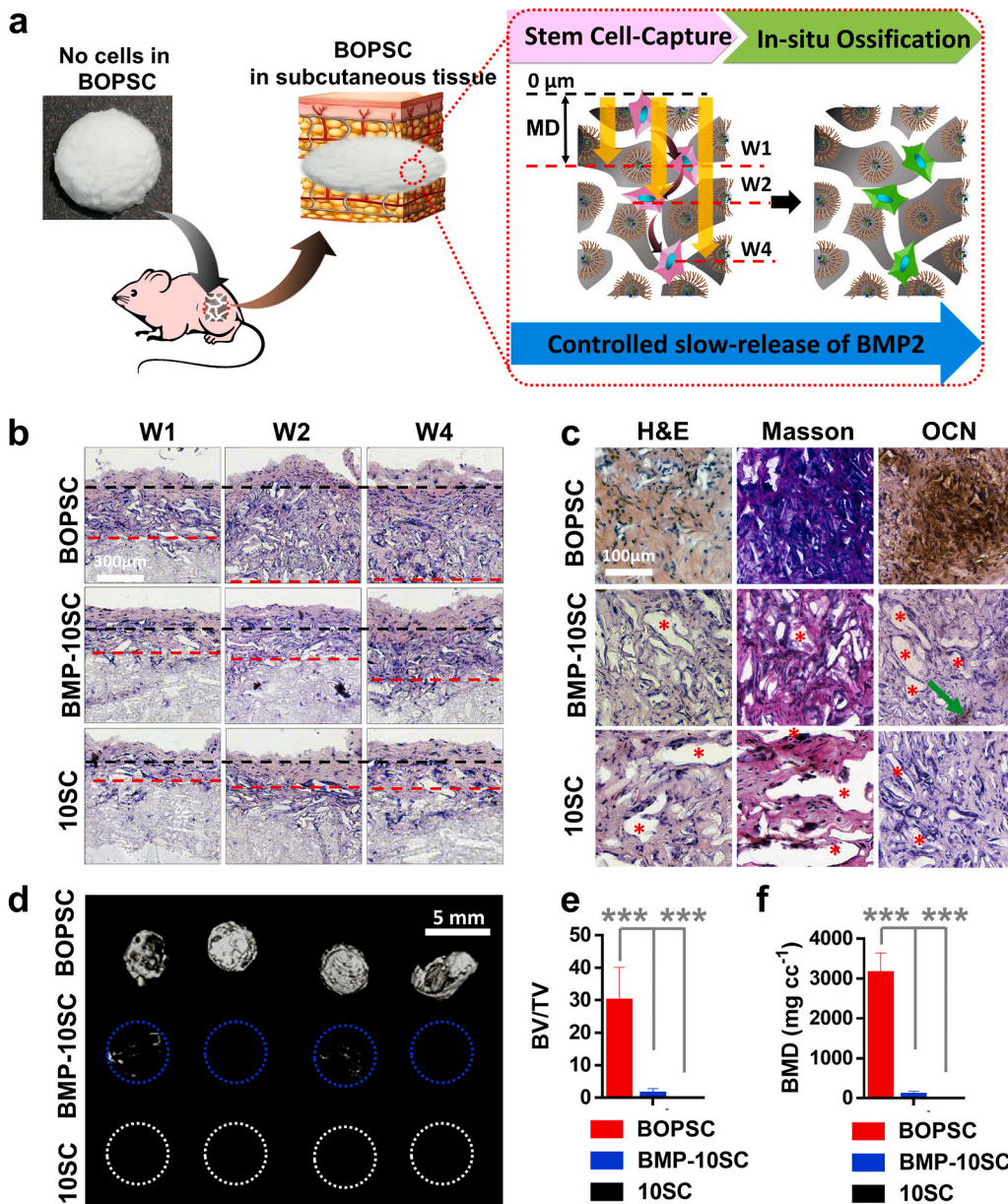


Fig. 7. *In vivo* ectopic bone formation of BOPSCs as a cell-free-platform. a) Schematic of *in vivo* cells-capture and *in-situ* osteogenic induction of BOPSCs accompanied with BMP2-release in mice. b) *In-vivo* cell-capture and migration of BOPSCs and control scaffolds implanted in subcutaneous tissue in Week 1 (W1), Week 2 (W2) and Week 4 (W4), respectively. The black lines indicate general interface of subcutaneous tissue and scaffolds. The red lines indicate general interface of captured cells in scaffolds and blank space of scaffolds. c) H&E, Masson and immunohistochemical OCN staining of BOPSCs, BMP-10SCs and 10SCs after implantation in mice for 6 months. The red stars indicate inner space without cell growth, and the green arrows indicate few OCN expression areas in BMP-10SCs. d) Reconstructed 3D micro-CT image, e) bone mineral density (BMD), and f) ratios of new bone volume to existing tissue volume (BV/TV) of BOPSCs, BMP-10SCs and 10SCs, respectively. Four parallel measurements were conducted for each sample in (d) and (e). ***p < 0.005.

distance (MD) to describe the migration ability of cells grown into internal space of scaffolds after cell-capture in subcutaneous tissues (schematic in Fig. 7a). In Fig. 7b, a large number of cells migrated from subcutaneous tissues (outer of scaffold) into internal space of scaffolds in 4 weeks. On account of sustaining BMP2-supply, BOPSCs showed best cell migration ability after cell-capture (MD > 600 μm) in 4 weeks; however, the MD of control scaffolds in week 4 was only 20%–40% of that of BOPSCs in 2 weeks, which explained the active BMP2 could improve biocompatibility of single polymer.

In addition to the migration, abundant captured cells and proliferated tissue occupied the internal blank space of BOPSCs and expressed excess collagen (Masson staining) and OCN (Fig. 7c). By contrast, some inner space without cell-growth (indicated by red stars in Fig. 7c) was found in BMP-10SCs and 10SCs, demonstrating their much weaker cell-capture capacity. Furthermore, the regenerated ectopic tissue of controls was not as strong as that of BOPSCs (Masson and OCN staining in Fig. 7c), even though few OCN-positive areas were observed in BMP-10SCs (indicated by green arrow in Fig. 7c).

Finally, micro-CT showed that the BOPSCs implants had significantly higher bone mineral density (BMD) of 3007 mg cc^{-1} and ratios of new bone volume to existing tissue volume (BV/TV) of 29.9% on month 6 (Fig. 7d–f), which was similar to that of hMSCs on commercial Bio-Oss collagen scaffolds for osteogenic induction, with BV/TV of 40% and BMD of 3350 mg cc^{-1} [61]. Conversely, scarce calcium deposition was found in BMP-10SCs with a BV/TV of only 1.24% and BMD of 80 mg cc^{-1} , which fell to zero in 10SCs. This was consistent with a previous report that SL-mediated PLGA microspheres could transport human bone mesenchymal stem cells (hBMSCs) as stem cell carriers into mice and successfully induce the differentiation of osteoblastic tissue [25]. This demonstrated that BOPSC is an effective 3D cell-free scaffold for *in vivo* stem-cell capture and *in situ* osteogenic induction, due to its sustained BMP2-supply.

4. Conclusions

To avoid the death and function-loss of exogenous cells after transplantation, we designed a novel cell-free scaffold based on biopolyesters for *in vivo* stem-cell capture and *in situ* osteogenic induction. Due to the assistance of SL, BMP2 was efficiently dispersed in the hydrophobic polyester material composed of a blend of PCL with PLGA-PEI, resulting in abundant and sustainably released BMP2. The optimized bioactive osteo-polyester scaffolds (BOPSCs), i.e. SBMP-10SCs, showed dual advantages of reasonable porous internal structure and sustained BMP2 release. BOPSCs led to much better capture, proliferation and osteogenic differentiation of mADSCs compared to traditional BMP-SCs with unmodified BMP2 or pure polyester scaffolds *in vitro* and *in vivo*. This system avoids the implantation of exogenous stem cells or osteoblasts, instead relying on the capture of stem cells and differentiation to osteoblasts on BOPSCs *in situ*, which successfully promoted allogeneic bone formation after 6 months of implantation in mice *in vivo*. Therefore, BOPSCs can autonomously capture stem cells and be applied as an advanced cell-free scaffold with sustained BMP2 supply for bone tissue engineering *in situ*.

CRedit authorship contribution statement

Mamatali Rahman: Investigation, preparation of scaffolds, reviewing. **Xue-Liang Peng:** Investigation, preparation of scaffolds, reviewing. **Xiao-Hong Zhao:** cell and animal experiment. **Hai-Lun Gong:** cell and animal experiment. **Xiao-Dan Sun:** Software. **Qiong Wu:** Conceptualization. **Dai-Xu Wei:** preparation of SL-BMP, scaffolds and cell and animal experiment, reviewing and Editing.

Declaration of competing interest

The authors declare no conflicts of interest.

Acknowledgements

M. Rahman and X. L. Peng contributed equally to this work. This work was supported by Grants from National Natural Science Foundation of China (Grant Nos. 31900950, 31670991 and 52072210), and National Key Research and Development Project of China (Grant No. 2018YFA0900100).

References

- [1] X. Du, D. Wei, L. Huang, M. Zhu, Y. Zhang, Y. Zhu, 3D printing of mesoporous bioactive glass/silk fibroin composite scaffolds for bone tissue engineering, *Mater. Sci. Eng. C Mater. Biol. Appl.* 103 (2019) 109731.
- [2] X.F. Cao, P.J. Song, Y.J. Qiao, P. Zhen, 3D printing of bone tissue engineering scaffolds, *Chin. J. Tissue Eng. Res.* 19 (25) (2015) 4076–4080.
- [3] Y.W. A, T.C. A, W.C. A, X.W. A, J.L. A, Y.C. A, Y.Y. A, Z.S. A, Q.Y. B, Y.Z. A, Release of VEGF and BMP9 from injectable alginate based composite hydrogel for treatment of myocardial infarction, *Bioact. Mater.* 6 (2) (2021) 520–528.
- [4] M.S. Namini, N. Bayat, R. Tajerian, S. Ebrahimi-Barough, M. Azami, S. Irani, S. Jangjoo, S. Shirian, J. Ai, A comparison study on the behavior of human endometrial stem cell-derived osteoblast cells on PLGA/HA nanocomposite scaffolds fabricated by electrospinning and freeze-drying methods, *J. Orthop. Surg. Res.* 13 (1) (2018) 63.
- [5] S. Shirian, S. Ebrahimi-Barough, H. Saberi, A. Norouzi-Javidan, S.M. Mousavi, M. A. Derakhshan, B. Arjmand, J. Ai, Comparison of capability of human bone marrow mesenchymal stem cells and endometrial stem cells to differentiate into motor neurons on electrospun poly(epsilon-caprolactone) scaffold, *Mol. Neurobiol.* 53 (8) (2016) 5278–5287.
- [6] A. Oryan, S. Alidadi, A. Moshiri, N. Maffulli, Bone regenerative medicine: classic options, novel strategies, and future directions, *J. Orthop. Surg. Res.* 9 (1) (2014) 18.
- [7] H.-W. Liu, D.-X. Wei, J.-Z. Deng, J.-J. Zhu, K. Xu, W.-H. Hu, S.-H. Xiao, Y.-G. Zhou, Combined antibacterial and osteogenic in situ effects of a bifunctional titanium alloy with nanoscale hydroxyapatite coating, *Artif. Cell Nanomed. Biotechnol.* 46 (sup3) (2018) S460–S470.
- [8] Q. Huang, Y. Liu, Z. Ouyang, Q. Feng, Comparing the regeneration potential between PLLA/Aragonite and PLLA/Vaterite pearl composite scaffolds in rabbit radius segmental bone defects, *Bioact. Mater.* 5 (4) (2020) 980–989.
- [9] H.A. Rather, R. Thakore, R. Singh, D. Jhala, S. Singh, R. Vasita, Antioxidative study of Cerium Oxide nanoparticle functionalised PCL-Gelatin electrospun fibers for wound healing application, *Bioact. Mater.* 3 (2) (2017) 201–211.
- [10] D.X. Wei, J.W. Dao, G.Q. Chen, A micro-ark for cells: highly open porous polyhydroxyalkanoate microspheres as injectable scaffolds for tissue regeneration, *Adv. Mater.* 30 (31) (2018) 1802273.
- [11] D.-X. Wei, J.-W. Dao, H.-W. Liu, G.-Q. Chen, Suspended polyhydroxyalkanoate microspheres as 3D carriers for mammalian cell growth, *Artif. Cell Nanomed. Biotechnol.* 46 (sup2) (2018) 473–483.
- [12] C. Chun-Yuan, P. Quoc-Hue, W. Xiao-Yu, C. Ting-Yu, C. Chien-Min, F. Peng-Hsiang, L. Yung-Chang, H. Ming-Fa, PLGA microspheres loaded with β -cyclodextrin complexes of epigallocatechin-3-gallate for the anti-inflammatory properties in activated microglial cells, *Polymers* 10 (5) (2018) 519.
- [13] P. Pei, D. Wei, M. Zhu, X. Du, Y. Zhu, The effect of calcium sulfate incorporation on physicochemical and biological properties of 3D-printed mesoporous calcium silicate cement scaffolds, *Microporous Mesoporous Mater.* 241 (2017) 11–20.
- [14] N. Xu, X. Ye, D. Wei, J. Zhong, Y. Chen, G. Xu, D. He, 3D artificial bones for bone repair prepared by computed tomography-guided fused deposition modeling for bone repair, *ACS Appl. Mater. Interfaces* 6 (17) (2014) 14952–14963.
- [15] L. Guomin, L.U. Tiancheng, J.I. Xuan, J. Wenyuan, L.I. Yalong, Z. Yian, L. Yungang, Preparation and osteogenic induction activity of CBD-BMP2-MP/PLGA 3D printed composite scaffolds, *Chem. J. Chin. Univ.* 40 (7) (2019) 1552–1560.
- [16] X. Liu, D. Wei, J. Zhong, M. Ma, J. Zhou, X. Peng, Y. Ye, G. Sun, D. He, Electrospun nanofibrous P(DLLA-CL) balloons as calcium phosphate cement filled containers for bone repair: *in vitro* and *in vivo* studies, *ACS Appl. Mater. Interfaces* 7 (33) (2015) 18540–18552.
- [17] G. Sun, D. Wei, X. Liu, Y. Chen, M. Li, D. He, J. Zhong, Novel biodegradable electrospun nanofibrous P(DLLA-CL) balloons for the treatment of vertebral compression fractures, *Nanomedicine* 9 (6) (2013) 829–838.
- [18] Y. Chen, M. Shafiq, M. Liu, M. Yosrey, X. Mo, Advanced fabrication for electrospun three-dimensional nanofiber aerogels and scaffolds, *Bioact. Mater.* 5 (4) (2020).
- [19] S.H. Han, M. Cha, Y.Z. Jin, K.M. Lee, J.H. Lee, BMP-2 and hMSC dual delivery onto 3D printed PLA-Biogel scaffold for critical-size bone defect regeneration in rabbit tibia, *Biomed. Mater.* 16 (2020) 015019.
- [20] Q. Yao, J.G. Cosme, T. Xu, J.M. Miszuk, P.H. Picciani, H. Fong, H. Sun, Three dimensional electrospun PCL/PLA blend nanofibrous scaffolds with significantly improved stem cells osteogenic differentiation and cranial bone formation, *Biomaterials* 115 (2017) 115–127.
- [21] M. Wang, P. Favi, X. Cheng, N.H. Golshan, K.S. Ziemer, M. Keidar, T.J. Webster, Cold atmospheric plasma (CAP) surface nanomodified 3D printed polylactic acid (PLA) scaffolds for bone regeneration, *Acta Biomater.* 46 (2016) 256–265.
- [22] Y. Hao, Y.W. Chen, X.L. He, F. Yang, Z.Y. Qian, Near-infrared responsive 5-fluorouracil and indocyanine green loaded MPEG-PCL nanoparticle integrated with dissolvable microneedle for skin cancer therapy, *Bioact. Mater.* 5 (3) (2020) 542–552.

- [23] S. Moeini, M.R. Mohammadi, A. Simchi, In-situ solvothermal processing of polycaprolactone/hydroxyapatite nanocomposites with enhanced mechanical and biological performance for bone tissue engineering, *Bioact. Mater.* 2 (3) (2017) 146–155.
- [24] S.K. Hedayati, A.H. Behraves, S. Hasannia, A.B. Saed, B. Akhondi, 3D printed PCL scaffold reinforced with continuous biodegradable fiber yarn: a study on mechanical and cell viability properties, *Polym. Test.* 83 (2020).
- [25] D.X. Wei, R.R. Qiao, J.W. Dao, J. Su, C.M. Jiang, X.C. Wang, M.Y. Gao, J. Zhong, Soybean lecithin-mediated nanoporous PLGA microspheres with highly entrapped and controlled released BMP-2 as a stem cell platform, *Small* 14 (22) (2018).
- [26] Y. Qian, X. Zhou, F. Zhang, T.G.H. Diekwisch, X. Luan, J. Yang, Triple PLGA/PCL scaffold modification including silver impregnation, collagen coating, and electrospinning significantly improve biocompatibility, antimicrobial, and osteogenic properties for orofacial tissue regeneration, *ACS Appl. Mater. Interfaces* 11 (41) (2019) 37381–37396.
- [27] J. Yang, Y. Li, T. Zhang, X. Zhang, Development of bioactive materials for glioblastoma therapy, *Bioact. Mater.* 1 (1) (2016) 29–38.
- [28] J. Kong, B. Wei, T. Groth, Z. Chen, L. Li, D. He, R. Huang, J. Chu, M. Zhao, Biomaterialization improves mechanical and osteogenic properties of multilayer-modified PLGA porous scaffolds, *J. Biomed. Mater. Res.* 106 (10) (2018) 2714–2725.
- [29] J.D. Conway, L. Shabtai, A. Bauernschub, S.C. Specht, BMP-7 versus BMP-2 for the treatment of long bone nonunion, *Orthopedics* 37 (12) (2014) e1049–e1057.
- [30] P. De Biase, R. Capanna, Clinical applications of BMPs, *Injury* 36 (3) (2005) S43–S46.
- [31] P.W. Kammerer, A.M. Pabst, M. Dau, H. Staedt, B. Al-Nawas, M. Heller, Immobilization of BMP-2, BMP-7 and alendronic acid on titanium surfaces: adhesion, proliferation and differentiation of bone marrow-derived stem cells, *J. Biomed. Mater. Res.* 108 (2) (2020) 212–220.
- [32] R. Chen, J. Yu, H.L. Gong, Y. Jiang, M. Xue, N. Xu, D.X. Wei, C. Shi, An easy long-acting BMP7 release system based on biopolymer nanoparticles for inducing osteogenic differentiation of adipose mesenchymal stem cells, *J. Tissue Eng. Regen. Med.* 14 (7) (2020) 964–972.
- [33] M. Dang, L. Saunders, X. Niu, Y. Fan, P.X. Ma, Biomimetic delivery of signals for bone tissue engineering, *Bone Res.* 6 (2018) 25.
- [34] E.H. Groeneveld, E.H. Burger, Bone morphogenetic proteins in human bone regeneration, *Eur. J. Endocrinol.* 142 (1) (2000) 9–21.
- [35] H. Zhang, F. Migneco, C.Y. Lin, S.J. Hollister, Chemically-conjugated bone morphogenetic protein-2 on three-dimensional polycaprolactone scaffolds stimulates osteogenic activity in bone marrow stromal cells, *Tissue Eng.* 16 (11) (2010) 3441–3448.
- [36] G. Chen, L. Yang, Y. Lv, Cell-free scaffolds with different stiffness but same microstructure promote bone regeneration in rabbit large bone defect model, *J. Biomed. Mater. Res.* 104 (4) (2016) 833–841.
- [37] D.E. Muylaert, J.O. Fledderus, C.V. Bouten, P.Y. Dankers, M.C. Verhaar, Combining tissue repair and tissue engineering; bioactivating implantable cell-free vascular scaffolds, *Heart* 100 (23) (2014) 1825–1830.
- [38] G. Matsumura, N. Isayama, S. Matsuda, K. Taki, Y. Sakamoto, Y. Ikada, K. Yamazaki, Long-term results of cell-free biodegradable scaffolds for in situ tissue engineering of pulmonary artery in a canine model, *Biomaterials* 34 (27) (2013) 6422–6428.
- [39] C. Woiciechowsky, A. Abbushi, M.L. Zenclussen, P. Casalis, J.P. Kruger, U. Freymann, M. Endres, C. Kaps, Regeneration of nucleus pulposus tissue in an ovine intervertebral disc degeneration model by cell-free resorbable polymer scaffolds, *J. Tissue Eng. Regen. Med.* 8 (10) (2014) 811–820.
- [40] F.G. Lyons, A.A. Al-Munajjed, S.M. Kieran, M.E. Toner, C.M. Murphy, G.P. Duffy, F. J. O'Brien, The healing of bony defects by cell-free collagen-based scaffolds compared to stem cell-seeded tissue engineered constructs, *Biomaterials* 31 (35) (2010) 9232–9243.
- [41] S.-T. Cheng, Z.-F. Chen, G.-Q. Chen, The expression of cross-linked elastin by rabbit blood vessel smooth muscle cells cultured in polyhydroxyalkanoate scaffolds, *Biomaterials* 29 (31) (2008) 4187–4194.
- [42] B. Arbez, J.D. Kun-Darbois, T. Convert, B. Guillaume, P. Mercier, L. Hubert, D. Chappard, Biomaterial granules used for filling bone defects constitute 3D scaffolds: porosity, microarchitecture and molecular composition analyzed by microCT and Raman microscopy, *J. Biomed. Mater. Res. B Appl. Biomater.* 107 (2) (2019) 415–423.
- [43] H.G. Sundararaghavan, R.B. Metter, J.A. Burdick, Electrospun fibrous scaffolds with multiscale and photopatterned porosity, *Macromol. Biosci.* 10 (3) (2010) 265–270.
- [44] V. Karageorgiou, D. Kaplan, Porosity of 3D biomaterial scaffolds and osteogenesis, *Biomaterials* 26 (27) (2005) 5474–5491.
- [45] F.C. Kung, Injectable collagen/RGD systems for bone tissue engineering applications, *Bio Med. Mater. Eng.* 29 (2) (2018) 241–251.
- [46] I. Bilem, P. Chevallier, L. Plawinski, E.D. Sone, M.C. Durrieu, G. Laroche, RGD and BMP-2 mimetic peptide crosstalk enhances osteogenic commitment of human bone marrow stem cells, *Acta Biomater.* 36 (2016) 132–142.
- [47] S. Wang, Y. Yang, G.L. Koons, A.G. Mikos, Z. Qiu, T. Song, F. Cui, X. Wang, Tuning pore features of mineralized collagen/PCL scaffolds for cranial bone regeneration in a rat model, *Mater. Sci. Eng. C Mater. Biol. Appl.* 106 (2020) 110186.
- [48] J.Y. Won, C.Y. Park, J.H. Bae, G. Ahn, C. Kim, D.H. Lim, D.W. Cho, W.S. Yun, J. H. Shim, J.B. Huh, Evaluation of 3D printed PCL/PLGA/beta-TCP versus collagen membranes for guided bone regeneration in a beagle implant model, *Biomed. Mater.* 11 (5) (2016), 055013.
- [49] S. Fu, P. Ni, B. Wang, B. Chu, L. Zheng, F. Luo, J. Luo, Z. Qian, Injectable and thermo-sensitive PEG-PCL-PEG copolymer/collagen/n-HA hydrogel composite for guided bone regeneration, *Biomaterials* 33 (19) (2012) 4801–4809.
- [50] K.S. Hwang, J.W. Choi, J.H. Kim, H.Y. Chung, S. Jin, J.H. Shim, W.S. Yun, C. M. Jeong, J.B. Huh, Comparative efficacies of collagen-based 3D printed PCL/PLGA/beta-TCP composite block bone grafts and biphasic calcium phosphate bone substitute for bone regeneration, *Materials* 10 (4) (2017).
- [51] Y. Hu, B. Feng, W. Zhang, C. Yan, Q. Yao, C. Shao, F. Yu, F. Li, Y. Fu, Electrospun gelatin/PCL and collagen/PCL scaffolds for modulating responses of bone marrow endothelial progenitor cells, *Exp. Ther. Med.* 17 (5) (2019) 3717–3726.
- [52] A. Mota, A. Sahebgadam Lotfi, J. Barzin, M. Hatam, B. Adibi, Z. Khalaj, M. Massumi, Human bone marrow mesenchymal stem cell behaviors on PCL/gelatin nanofibrous scaffolds modified with A collagen IV-derived RGD-containing peptide, *Cell J* 16 (1) (2014) 1–10.
- [53] S. Pitjamt, K. Thunsiri, W. Nakkiew, T. Wongwichai, P. Pothacharoen, W. Wattanutchariya, The possibility of interlocking nail fabrication from FFF 3D printing PLA/PCL/HA composites coated by local silk fibroin for canine bone fracture treatment, *Materials* 13 (7) (2020).
- [54] C.L. Wang, F. Xiao, C.D. Wang, J.F. Zhu, C. Shen, B. Zuo, H. Wang, Li, X.Y. Wang, W.J. Feng, Z.K. Li, G.L. Hu, X. Zhang, X.D. Chen, Gremlin2 suppression increases the BMP-2-induced osteogenesis of human bone marrow-derived mesenchymal stem cells via the BMP-2/smad/runx2 signaling pathway, *J. Cell. Biochem.* 118 (2) (2017) 286–297.
- [55] M. Tandon, K. Gokul, S.A. Ali, Z. Chen, J. Lian, G.S. Stein, J. Pratap, Runx2 mediates epigenetic silencing of the bone morphogenetic protein-3B (BMP-3B/GDF10) in lung cancer cells, *Mol. Canc.* 11 (2012) 27.
- [56] M. Luna-Luna, S. Criales-Vera, D. Medina-Leyte, M. Diaz-Zamudio, A. Flores-Zapata, D. Cruz-Robles, M. Lopez-Meneses, S. Olvera-Cruz, S. Ramirez-Marroquin, C. Flores-Castillo, J.M. Fragoso, E. Carreon-Torres, J. Vargas-Barron, G. Vargas-Alarcon, O. Perez-Mendez, Bone morphogenetic protein-2 and osteopontin gene expression in epicardial adipose tissue from patients with coronary artery disease is associated with the presence of calcified atherosclerotic plaques, *Diabetes Metab. Syndr. Obes.* 13 (2020) 1943–1951.
- [57] K. Yamawaki, K. Matsuzaka, E. Kokubu, T. Inoue, Effects of epidermal growth factor and/or nerve growth factor on Malassez's epithelial rest cells in vitro: expression of mRNA for osteopontin, bone morphogenetic protein 2 and vascular endothelial growth factor, *J. Periodontol. Res.* 45 (3) (2010) 421–427.
- [58] D.D. Dou, G. Zhou, H.W. Liu, J. Zhang, M.L. Liu, X.F. Xiao, J.J. Fei, X.L. Guan, Y. B. Fan, Sequential releasing of VEGF and BMP-2 in hydroxyapatite collagen scaffolds for bone tissue engineering: design and characterization, *Int. J. Biol. Macromol.* 123 (2019) 622–628.
- [59] H. Koyama, O. Nakade, T. Saitoh, T. Takuma, T. Kaku, Evidence for the involvement of bone morphogenetic protein-2 in phenytoin-stimulated osteocalcin secretion in human bone cells, *Arch. Oral Biol.* 45 (8) (2000) 647–655.
- [60] B.L. Foster, M. Ao, C. Willoughby, Y. Soenjaya, E. Holm, L. Lukashova, A.B. Tran, H.F. Wimer, P.M. Zerfas, F.H. Nociti Jr., K.R. Kantovitz, B.D. Quan, E.D. Sone, H. A. Goldberg, M.J. Somerman, Mineralization defects in cementum and craniofacial bone from loss of bone sialoprotein, *Bone* 78 (2015) 150–164.
- [61] Q. He, S. Yang, X. Gu, M. Li, C. Wang, F. Wei, Long noncoding RNA TUG1 facilitates osteogenic differentiation of periodontal ligament stem cells via interacting with Lin28A, *Cell Death Dis.* 9 (5) (2018) 455.